Sustainable Chemical Engineering
https://ojs.wiserpub.com/index.php/SCE/

Research Article

Magneto-Radiative Nanofluid Flow over a Stretching Permeable Sheet with Heat Generation and Slip Boundary Effects: Homotopy Perturbation Method

Babulal Talukdar[1], Gopinath Mandal[2*]

[1]Department of Mathematics, Saheed Nurul Islam Mahavidyalaya, North 24 Parganas, 743286, West Bengal, India
[2]Siksha-Satra, Sriniketan, Visva-Bharati (A Central University of National Importance), Birbhum District, West Bengal, 731236, India
E-mail: gopi_math1985@rediffmail.com

Received: 14 November 2024; **Revised:** 3 December 2024; **Accepted:** 10 December 2024

Abstract: This study explores the nanofluid's flow and heat transfer over a stretching surface, considering the influence of a Darcy-Forchheimer porous medium and an external magnetic field. Moreover, thermal radiation effects, heat source/sink impacts, and second-order slip boundary conditions are incorporated into the problem. The nanofluid is developed by dispersing copper (Cu) or alumina (Al_2O_3) nanoparticles into a water (H_2O) base fluid. Appropriate similarity transformations are applied to convert the controlling equations into ordinary differential equations. This study's novelty lies in the homotopy perturbation method (HPM) used to solve the resultant highly nonlinear coupled differential equations analytically. The effects of several relevant factors are thoroughly examined using graphs and tables for skin friction, temperature, velocity, and heat transfer rate. The findings demonstrate that raising the magnetic parameter significantly increases the skin friction coefficient while lowering the heat transmission rate. The results show that raising the volume percentage of copper and alumina nanoparticles enhances the skin friction coefficient. Nusselt numbers are found to reduce with thermal radiation and thermal slip parameters for both nanofluid flows. This investigation has applications in paper manufacturing, metal sheet cooling, and crystal growth. In high-temperature industrial applications, radiation heat transfer research is critical.

***Keywords*:** nanofluid, stretching surface, darcy-forchheimer, thermal radiation, magnetic field, second order velocity slip, thermal slip, homotopy perturbation method (HPM)

Nomenclature

A, A_1	First order velocity slip parameter
B, B_1	Second order velocity slip parameter
Br	Brinkman number
C_p	Specific heat, ($J \cdot Kg^{-1} \cdot K^{-1}$)
C_f	Coefficient of skin-friction
F*	Darcy-Forchheimer medium
Fr	Forchheimer number
L	Reference length

DOI: https://doi.org/10.37256/sce.6220256074

k*	Porous medium
M	Magnetic parameter
Nu_x	Nusselt number
P_r	Prandtl number
P	Porous parameter
q_r	Thermal radiative heat flux ($W \cdot m^{-2}$)
Q	heat source/sink joule (J)
R_d	thermal radiation parameter
Re	Reynolds number
R	heat source/sink parameter
Re_x	Local Reynolds number
C_f	Coefficient of heat transfer
S	Suction/injection parameter
T_w	Temperature of surface (K)
T	Temperature of fluid (K)
$T\infty$	Temperature at free-stream (K)
$u_{w(x)}$	shrinking surface velocity (m/s)
u, v	Fluid velocity components (m/s)
x, y	Cartesian coordinates

Greek letters

ϕ_0	Nanoparticles's volume fraction
η	Similarity variable
K*	Coefficient of mean absorption (m^{-1})
k	Thermal conductivity ($W \cdot m^{-1} \cdot K$)
μ	Viscosity ($kg \cdot m^{-1} \cdot s^{-1}$)
ρ	Density of fluid ($kg \cdot m^{-3}$)
ρ(Cp)	Heat capacity ($J \cdot K^{-1} \cdot m^{-3}$)
ξ	Stretching/shrinking parameter
$\theta(\eta)$	Dimensionless temperature

Subscripts

f	Base fluid
nf	Nanofluid

1. Introduction

Due to its many applications in engineering and industry, heat transfer improvement over stretching or shrinking surfaces has attracted much interest lately. The study of flow and heat transfer of viscous fluid over a continuously stretching surface in an otherwise quiescent fluid medium has attracted considerable attention. This is owing to the applications of such a problem in many important practical applications in engineering and industrial processes, such as the extrusion of a polymer in a melt-spinning process, continuous casting of metals, the aerodynamic extrusion of plastic sheets, the cooling of metallic sheets or electronic chips and many others. The resulting flow over a continuous stretching surface extruded from a slit may be modelled as a boundary layer developing away from silt. Following the pioneering work of Sakiadis, most theoretical investigations in this field described fluid flow and heat transfer near the continuous stretching surface with the aid of similarity solutions to the boundary layer equations.[1] Later, Tsou et al. made an experimental and theoretical study, which experimentally determined the heat transfer rates for certain Prandtl numbers and confirmed that the flow field obtained by Sakiadis was broadly realized experimentally.[2] In recent years,

the boundary layer flow due to a shrinking sheet has attracted many researchers because of its useful applications. Later, Crane considered the flow problem over a linearly stretching sheet in an ambient fluid and gave a similar solution in closed analytical form for the steady two-dimensional problem.[3] Shrinking surfaces is also a common application of shrinking sheet problems in engineering and industries. Shrinking film is very useful in packaging bulk products because it can be unwrapped easily with adequate heat. Heat transfer fluids, such as water, paraffin oil, diathermic oil, ethylene glycol, naphthenic mineral oil, vegetable oil, etc., are used as cooling fluids in most applications. Mandal and Pal investigated shrinking or stretching surfaces under various conditions.[4-7]

Heat transmission is minimized by these typical fluids' low thermal conductivity. Therefore, introducing nanoparticles into the base fluid to produce a nanofluid combination is a novel way to enhance heat transmission in fluids. Choi and Eastman were the ones who first introduced it.[8] Compared to ordinary fluids, nanofluids have substantially more excellent thermal conductivity. Therefore, nanofluids are widely employed for many different applications, including biomedicine, electronic device cooling, nuclear cooling, and cooling of automobiles and machinery. As a result, several researchers have used numerical and experimental methods to examine the behaviours and characteristics of nanofluids in various contexts. For instance, a mathematical model of nanofluids has been presented by Tiwari and Das to study the behaviour of nanofluids while considering the impacts of solid volume fractions of nanoparticles.[9] The homotopy perturbation approach was used to solve the governing equations. Magyari and Keller investigated heat transfer and boundary layer flow caused by an exponentially stretched continuous surface.[10] Zhang et al. demonstrated that the suspension of hybrid nanoparticles caused a thermal increase in a porous media.[11] Sajjan et al. worked with ternary nanoparticles of different densities, morphologies, and conductivity characteristics in their experiments.[12] Rehman et al. addressed the significance of Casson dusty nanofluid in the presence of Darcy-Forchheimer medium, a magnetic field subject to a stretched surface.[13] Kumar et al. concentrated on linear and quadratic convection for hybrid nanoparticles.[14] Raju et al. investigated the nonlinear motions of ternary hybrid nanofluids in thermally radiated expanding or contracting permeable Darcy Walls.[15]

The majority of the studies above have made use of the no-slip condition. However, when fluid flows in the micro electro mechanical system (MEMS), the no-slip requirement at the solid-fluid interface is no longer relevant. Mixed convection boundary layer flow with temperature slip boundary conditions in a porous media was examined by Merkin et al.[16] Numerous scholars have studied the fluid flow for various characteristics in a slip flow regime.[17-24] To discover the analytical solution for a nonlinear ordinary and partial differential equation or a linked nonlinear system of partial differential equations, the Homotopy perturbation technique (HPM) was created lately. Many scholars have used this method as an example in their separate fields of study since it simplifies and expedites the computation of analytical findings compared to other analytical techniques. He did the ground breaking work by the help of homotopy perturbation method.[25-27] The motion of a nanofluid's thin film with heat transfer was solved using the HPM method by Nabil et al.[28] The homotopy perturbation method for couple stresses effect on MHD peristaltic flow of a non-Newtonian nanofluid was also used by Mohamed et al.[29] Several researchers have used this technique in various fields of mathematical and engineering studies since it simplifies the calculations of analytical results compared to other analytical methods.[30-32]

My goal in this work is to examine the boundary layer of Cu-water and Al_2O_3-water nanofluid flow and heat transfer caused by an exponentially expanding permeable sheet when magnetic field, thermal radiation, second-order velocity, and thermal boundary conditions are present. The governing PDEs were reduced to a set of nonlinear ODEs using the proper similarity transformations. HPM is used to provide analytical solutions for the momentum and energy equations. Analytical and pictorial discussions on the effects of the problem's numerous parameters were held to manage the fluid's motion.

The novelty and primary contribution of this work is

(1) To examine the effects of magnetic field, thermal radiation, and heat generation in the existence of second-order velocity slip and thermal conditions at the surface of the exponentially stretching surface.

(2) To compare the effectiveness of two types of flow models (Cu-water and Al_2O_3-water) by analyzing velocity, temperature, skin friction coefficient, and Nusselt number over an exponential stretching sheet.

(3) To analyze the Homotopy Perturbation Method for finding stable solutions for transformed ordinary differential equations.

2. Mathematical formulation

The study examines a continuous, incompressible nanofluid slip flow boundary layer that passes an exponentially permeable stretching sheet through a Darcy-Forchheimer porous medium. The flow velocity of the nanofluid is considered to be $\overline{u}$ in the x direction (see Figure 1). Alternatively, velocity $\overline{v}$ in the y direction, normal to the x-coordinate (Figure 1). $\overline{u}_w(x) = \overline{u}_0 e^{x/L}$ is the velocity of the deformable surface and $\overline{v}_w(x) = \overline{v}_0 e^{x/2L}$ ($\overline{v}_0 < 0$ indicates mass removal, $\overline{v}_0 > 0$ indicates mass injection) is the constant mass flux velocity. $\xi > 0, < 0, = 0$ denotes a stretched surface, a shrinking surface, and a stationary surface, respectively. Additionally, the flow zone plane $y = 0$ is generally controlled by an applied magnetic field $\overline{B} = \overline{B}_0 e^{x/2L}$ of constant strength $\overline{B}_0$. The impressed electric and induced magnetic fields are ignored here due to low Renold's number. A changing wall temperature is assumed so that $\overline{T}_w = \overline{T}_\infty + \overline{T}_0 e^{x/2L}$ with constant $\overline{T}_0 > 0$, $\left(\overline{T}_w > \overline{T}_\infty\right)$ indicates a heated sheet for supporting flow and $\overline{T}_0 < 0$, $\left(\overline{T}_w < \overline{T}_\infty\right)$ indicates a cooled sheet for opposing flow. The thermal conductivity of the nanofluid is expected to change linearly with temperature, $\overline{T}$. As temperature, nanoparticle type, pressure, etc., increase, the thermal characteristics of the nanofluid alter dramatically. Lastly, the Rosseland approximation is used for the radiation effects, radiative heat transfer is considered, and the nanofluid is considered optically thick. The base fluid and the nanoparticle are assumed to be in thermal equilibrium. The linked boundary layer continuity, momentum, and energy equations, including boundary conditions, are constructed as follows under all of the assumptions above:[21]

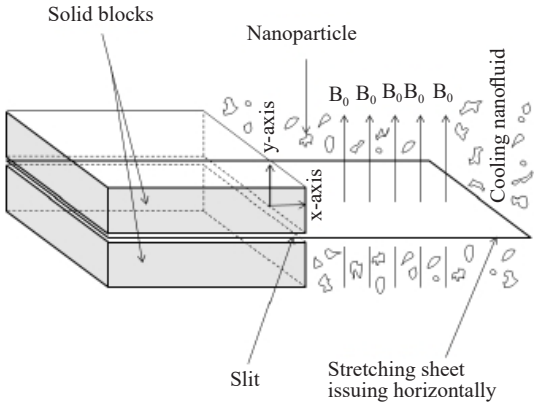

Figure 1. Flow configuration

$$\frac{\partial \overline{u}}{\partial x} + \frac{\partial \overline{v}}{\partial y} \tag{1}$$

$$\overline{u}\frac{\partial \overline{u}}{\partial x} + \overline{v}\frac{\partial \overline{v}}{\partial y} = \frac{\mu_{nf}}{\rho_{nf}}\frac{\partial^2 \overline{u}}{\partial y^2} - \frac{\mu_{nf}}{\rho_{nf}}\frac{\overline{u}}{\mathrm{k}^*} - \frac{F^*}{\sqrt{\mathrm{K}^*}}\overline{u}^2 - \frac{\sigma_{nf}\overline{B}^2}{\rho_{nf}}\overline{u} \tag{2}$$

$$\overline{u}\frac{\partial T}{\partial x} + \overline{v}\frac{\partial T}{\partial y} = \frac{\kappa_{nf}}{\left(\rho C_p\right)_{nf}}\frac{\partial^2 T}{\partial y^2} - \frac{1}{\left(\rho C_p\right)_{nf}}\frac{\partial \overline{q}_r}{\partial y} + \frac{\overline{Q}}{\left(\rho C_p\right)_{nf}}\left(\overline{T} - \overline{T}_\infty\right), \tag{3}$$

subject to the appropriate boundary conditions:

$$\overline{u} = \overline{u}_w + \overline{u}_{slip},\ \overline{v} = \overline{v}_w,\ \overline{T} = \overline{T}_w(x) + C_1\frac{\partial \overline{T}}{\partial y}\ \text{at}\ y = 0, \tag{4}$$

$$\overline{u} \to 0,\ \overline{T} \to \overline{T}_{\infty} \text{ as y} \to \infty \tag{5}$$

The heat production rate constant $\overline{Q} = \overline{Q}_0 e^{x/L}$, and the temperature slip factor that depends on x is $C_1 = ce^{x/2L}$.[33,34] The $\overline{u}_{\text{slip}}$ has the following form:

$$\overline{u}_{\text{slip}} = \frac{2}{3}\left(\frac{3-\alpha l^3}{\alpha} - \frac{3}{2}\frac{1-l^2}{\text{K}_n}\right)\gamma_0 \frac{\partial \overline{u}}{\partial y} - \frac{1}{4}\left(l^4 + \frac{2}{\text{K}_n^2}\left(1-l^2\right)\right)\gamma_0^2 \frac{\partial^2 \overline{u}}{\partial y^2} = A_1 \frac{\partial \overline{u}}{\partial y} + B_1 \frac{\partial^2 \overline{u}}{\partial y^2} \tag{6}$$

Where $l = \min\left(\frac{1}{\text{K}_n},\ 1\right)$, $\alpha(0 \le \alpha \le 1)$ is the momentum accomodation co-efficient and $\gamma_0(>0)$(Kn) is the mean free path. Hence for any Kundsen number (Kn), $A_1 > 0$ and $B_1 < 0$. When using the Rosseland approximation (Magyari and Pantokratoras) to gray/optical thick media, the formula for the net radiation heat flow $\overline{q}_r$ may be used to simulate an isotropic diffusion process.[35]

$$\overline{q}_r = -\frac{4\sigma^*}{3\text{K}^*}\frac{\partial \overline{T}^4}{\partial y} \tag{7}$$

Here $\overline{T}^4$ can be expanded as Taylors series about $\overline{T}_{\infty}$ and neglecting the higher order terms, we have

$$\overline{T}^4 \approx 4\overline{T}_{\infty}^3 \overline{T} - 3\overline{T}_{\infty}^4, \tag{8}$$

To non-dimensionalize those above, the Eqs. (1)-(5), the following similarity variables are introduced:[36]

$$\psi = e^{x/2L}\sqrt{2v_f L\overline{u}_0}\, g(\eta),\ \overline{u} = \frac{\partial \psi}{\partial y},\ \overline{v} = \frac{\partial \psi}{\partial x},\ \theta(\eta) = \frac{\overline{T}-\overline{T}_{\infty}}{T_w - T_{\infty}},\ \eta = ye^{x/2L}\sqrt{\frac{\overline{u}_0}{2v_f L}}, \tag{9}$$

With transform Eqs. (2)-(3) into the non-dimensional subsequent equations, before gratifying Eq. (1)

$$\left(\frac{\mu_{nf}/\mu_f}{\rho_{nf}/\rho_f}\right)g''' + gg'' - 2g'^2 - \left(\frac{\mu_{nf}/\mu_f}{\rho_{nf}/\rho_f}\right)Pg' - F_r g'^2 - \left(\frac{\sigma_{nf}/\sigma_f}{\rho_{nf}/\rho_f}\right)Mg' = 0, \tag{10}$$

$$\text{or, } g''' + A_4 gg'' - E_1 g'^2 - F_1 g' = 0, \tag{11}$$

$$\frac{1}{P_r}\left(\frac{\kappa_{nf}}{\kappa_f} + R_d\right)\theta'' + \frac{\left(\rho C_p\right)_{nf}}{\left(\rho C_p\right)_f}\left(g\theta' - g'\theta\right) + R\theta = 0, \tag{12}$$

$$\text{or, } \theta'' + L_1\left(g\theta' - g'\theta\right) + L_2\theta = 0, \tag{13}$$

Where A_4, E_1, F_1, L_1, and L_2 are constants (see in the Appendix).
With subjected boundary conditions:

$$g(0) = S,\ g'(0) = \xi + Ag''(0) + Bg'''(0),\ \theta = 1 + C\theta' \text{ at } \eta = 0 \tag{14}$$

$$g' \to 0,\ \theta \to 0 \text{ as } \eta \to \infty \tag{15}$$

In this case, we take into account $\xi = 1$ due to the stretching sheet. Additionally, the following new physical parameters are defined: wall mass flux transfer parameter $S\left(S = -\overline{v}_0\sqrt{\frac{v_f \overline{u}_0}{2L}}\right)$, first order velocity slip parameter $A\left(A = A_1\sqrt{\frac{\overline{u}_0}{2v_f L}}e^{x/2L}\right)$, second order velocity slip parameter $B\left(B = B_1\sqrt{\frac{\overline{u}_0}{2v_f L}}e^{x/2L}\right)$, thermal slip parameter $C\left(C = C_1\sqrt{\frac{\overline{u}_0}{2v_f L}}\right)$ Magnetic field parameter $M\left(M = \frac{\sigma_f B_0^2 L}{\overline{u}_0 \rho_f}\right)$, porosity parameter $P\left(P = \frac{v_f}{\overline{u}_0 k^*}\right)$, Forchheimer number $F\left(F_r = \frac{\chi F^*}{\sqrt{k^*}}\right)_r$, Prandtl number $P_r\left(P_r = \frac{\left(\mu C_p\right)_f}{\kappa_f}\right)$, thermal radiation parameter $R_d\left(R_d = \frac{16\sigma^* \overline{T}_\infty^3}{3k_f K^*}\right)$, heat generation $R\left(R = \frac{2\overline{Q}_0 L}{\overline{u}_0\left(\rho C_p\right)_f}\right)$. The thermophysical properties of nanoparticle and base fluids as are provided in Table 1.

Table 1. Thermophysical properties of nanoparticle and base fluids as follows[38]

Physical properties	Water	Cu	Al_2O_3
C_p (J/kgK)	4,179	385	765
ρ (kg/m^3)	997.1	8,933	4,250
κ (w/mK)	0.613	400	40
σ (Ω/m)	0.05	59.6×10^4	35×10^4
μ (Pa·s)	10^{-3}		

To have similar solutions, the quantities A and B must be constants and it is possible if the mean free path of the nanoparticles γ_0 is proportional to $e^{x/2L}$. We therefore assume $\gamma_0 = de^{-x/2L}$. Where d is the proportionality constant.

Physical characteristics of nanofluid density ρ_{nf}, heat capacitance $\left(\rho C_p\right)_{nf}$, thermal conductivity K_{nf}, electrical conductivity σ_{nf}, and dynamic viscosity μ_{nf}, are as follows:[37]

$$\rho_{nf} = \left(1-\phi_0\right)\rho_f + \phi_0\rho_s,\ \left(\rho C_p\right)_{nf} = \left(1-\phi_0\right)\left(\rho C_p\right)_f + \phi_0\left(\rho C_p\right)_s,$$

$$\kappa_{nf} = \kappa_f\left[\frac{\kappa_s + 2\kappa_f - 2\phi_0\left(\kappa_f - \kappa_s\right)}{\kappa_s + 2\kappa_f + 2\phi_0\left(\kappa_f - \kappa_s\right)}\right],\ \sigma_{nf} = \frac{\kappa_{nf}}{\left(\rho C_p\right)_{nf}},\ \mu_{nf} = \frac{\mu_f}{\left(1-\phi_0\right)^{2.5}},$$

3. Solution with homotopy perturbation method

The homotopy perturbation method (HPM) is a spectrum extension method used in a solution of both non-linear partial and ordinary differential equations. The method appoints a homotopy modify to generate an approximate series solution of differential equations. According to the HPM, the homotopy form of Eqs. (11) and (13) are constructed as follows:[38]

$$\left(1-q\right)\left(g''' - F_1 g'\right) + q\left[g''' + A_4 g g'' - E_1 g'^2 - F_1 g'\right] = 0 \tag{16}$$

$$\left(1-q\right)\left(\theta'' + L_2\theta\right) + q\left[\theta'' + L_1\left(g\theta' - g'\theta\right) + L_2\theta\right] = 0 \tag{17}$$

We consider g and θ as following:

$$g = g_0 + qg_1 + q^2 g_2 + \ldots \tag{18}$$

$$\theta = \theta_0 + q\theta_1 + q^2\theta_2 + \ldots \tag{19}$$

Substituting Eq. (18) into Eq. (16) and equating the like terms and neglecting higher order of q, we find

$$g_0''' - F_1 g_0' = 0 \tag{20}$$

$$g_1''' - F_1 g_1' + A_4 g_0 g_0'' - E_1 g_0'^2 = 0 \tag{21}$$

The corresponding boundary conditions are

$$g_0(0) = S,\ g_0'(0) = \xi + Ag_0'' + Bg_0'''(0),\ g_0'(\infty) = 0 \tag{22}$$

$$g_1(0) = S,\ g_1'(0) = \xi + Ag_1'' + Bg_1'''(0),\ g_1'(\infty) = 0 \tag{23}$$

Substituting Eq. (19) into Eq. (17) and neglecting higher order of q, we find

$$\theta_0'' + L_2\theta_0 = 0 \tag{24}$$

$$\theta_1'' + L_2\theta_1 + L_1 g_0\theta_0' - L_1 g_0'\theta_0 = 0 \tag{25}$$

The corresponding boundary conditions are

$$\theta_0(0) = 1 + C\theta_0'(0),\ \theta_0(\infty) = 0 \tag{26}$$

$$\theta_1(0) = C\theta_1'(0),\ \theta_1(\infty) = 0 \tag{27}$$

Solving Eqs. (20)-(21) and (24)-(25) with boundary conditions (22)-(23) and (26)-(27) respectively, We have

$$g_0 = d_1 + d_2 e^{-\sqrt{F_1}\eta} + d_3 e^{\sqrt{F_1}\eta} \tag{28}$$

$$g_1 = d_4 + d_5 e^{-\sqrt{F_1}\eta} + d_6 e^{\sqrt{F_1}\eta} - h_{10}\eta e^{-\sqrt{F_1}\eta} - h_{11}\eta e^{\sqrt{F_1}\eta} + h_{12}e^{-2\sqrt{F_1}\eta} - h_{13}e^{2\sqrt{F_1}\eta} + h_{14}\eta \tag{29}$$

$$g(\eta) = g_0(\eta) + qg_1(\eta) \tag{30}$$

$$\theta_0 = d_7 \cos\left(\sqrt{L_2}\eta\right) + d_8 \sin\left(\sqrt{L_2}\eta\right) \tag{31}$$

$$\theta_1 = d_9 \cos\left(\sqrt{L_2}\eta\right) + d_{10} \sin\left(\sqrt{L_2}\eta\right) d_{25}\eta \cos\left(\sqrt{L_2}\eta\right) + d_{26}\eta \sin\left(\sqrt{L_2}\eta\right)$$

$$+ d_{27} e^{-\sqrt{F_1}\eta} \cos\left(\sqrt{L_2}\eta\right) + d_{29} e^{\sqrt{F_1}\eta} \cos\left(\sqrt{L_2}\eta\right) + d_{30} e^{\sqrt{F_1}\eta} \sin\left(\sqrt{L_2}\eta\right) \tag{32}$$

$$\theta(\eta) = \theta_0(\eta) + q\theta_1(\eta) \tag{33}$$

The constant co-efficient, can be calculated using boundary condition $\eta = \infty$ were replaced by those at $\eta = 5$ in accordance with standard practice in the boundary layer analysis. If $q \to 1$, we find the approximate solution of Eqs. (16) and (17). The constant coefficients are defined in the Appendix.

4. Physical quantities

The physical characteristics of interest, such the shear stress coefficient, drag force, and heat flux, have many uses from a scientific and engineering standpoint. According to Mandal,[37] the following are the mathematical equations for the material important quantities in flow and heat transfer of nanofluid flow skin-friction coefficient *Cf* and Nusselt Number Nu_x:

$$C_f = \frac{\mu_{nf}}{\rho_f \overline{u}_w^2}\left(\frac{\partial \overline{u}}{\partial y}\right)_{y=0}, \; Nu_x = \frac{\left[\kappa_{nf}\left(-\frac{\partial \overline{T}}{\partial y}\right) + \frac{4\sigma^*}{3\mathrm{K}^*}\left(-\frac{\partial \overline{T}^4}{\partial y}\right)\right]_{y=0}}{\kappa_f\left(\overline{T}_f - \overline{T}_\infty\right)} \tag{34}$$

Finally the skin-friction coefficient and local Nusselt number can be expressed as

$$(2\mathrm{Re})^{1/2} e^{x/L} C_f = \frac{\mu_{nf}}{\mu_f} g''(0), \; \sqrt{2L/x}\,\mathrm{Re}_x^{-1/2} Nu_x = -\left(\frac{\kappa_{nf}}{\kappa_f} + R_d\right)\theta'(0) \tag{35}$$

Where $\mathrm{Re} = \overline{u}_w(x)L/\nu_f$ is the Reynolds number and $\mathrm{Re}_x = \overline{u}_w(x)x/\nu_f$ is the local Renolds number.

Table 2. Comparison of Skin friction with different values of parameters

S	*M*	(Cu-water nanofluid)	(Al_2O_3-water nanofluid)
2.0	0.1	2.401667595	1.999551177
2.5	0.1	2.609520197	2.153046131
3.0	0.1	2.817372322	2.306540966
3.5	0.1	3.025225401	2.460036512
2.0	0.1	2.401667595	1.999551177
2.0	0.2	2.332629681	1.955947161
2.0	0.3	2.271768570	1.917825580
2.0	0.4	2.217599630	1.884155512

Table 3. Comparison of Skin friction with different values of parameters

P	φ_0	(Cu-water nanofluid)	(Al_2O_3-water nanofluid)
1.0	0.1	2.401667595	1.999551177
2.0	0.1	1.962006450	1.728705525
3.0	0.1	1.758499861	1.608521223
4.5	0.1	1.636095762	1.536658645
1.0	0.01	2.038030863	1.986933589
1.0	0.02	2.092796564	1.993190527
1.0	0.03	2.143735409	1.998144269
1.0	0.04	2.234545469	2.004297256

Table 4. Change of Nusselt number with different values of parameters

P_r	R_d	(Cu-water nanofluid)	(Al_2O_3-water nanofluid)
0.3	0.1	0.528959930	0.530804753
0.62	0.1	0.903821111	0.907984376
0.8	0.1	1.125456929	1.131138802
1.0	0.1	1.382516503	1.390124083
0.62	0.1	0.903821111	0.907984376
0.62	0.2	0.855118275	0.858488977
0.62	0.3	0.812708914	0.815452039
0.62	0.4	0.775443733	0.777682662

Table 5. Change of Nusselt number with different values of parameters

R	C	(Cu-water nanofluid)	(Al_2O_3-water nanofluid)
0.1	0.1	0.903821111	0.907984376
0.2	0.1	0.868944287	0.873060882
0.3	0.1	0.834070802	0.838339388
0.4	0.1	0.803909004	0.808961153
0.1	0.1	0.903821111	0.907984376
0.1	0.2	0.883838236	0.888033509
0.1	0.3	0.864540398	0.868761897
0.1	0.4	0.845895946	0.850138843

5. Results and discussion

This part explores the significance of calculated findings for the current study and evaluates the solutions in the nanofluid. Furthermore, Tables 2-5 provide a tabular study of particular factors about the skin-friction coefficient and the

local Nusselt number, while Figures 2 show velocity and temperature profile graphs. The default values of the governing parameters are $\phi_0 = 0.1$, $Fr = 1.0$, $R_d = 0.1$, $M = 0.1$, $S = 2.0$, $A = 0.1$, $B = -0.1$, $C = 0.1$, $R = 0.1$, $P_r = 0.62$. Table 2 shows the skin-friction coefficients for Cu-water and Al_2O_3 -water nanofluids for various values of the suction parameter and magnetic field parameter *M*. Skin friction increases with increasing suction parameter *S* but decreases with magnetic parameter *M* for both types of nanofluids. Table 3 further demonstrates that the skin friction coefficient decreases with the porosity parameter *P* in both types of nanofluids. Skin friction in Cu-water and Al_2O_3 nanofluid are increased by nanoparticle volume fraction. Table 4 is designed to determine the Nusselt number for Cu-water and Al_2O_3 -water nanofluids for different values of Prandtl number P_r and thermal radiation parameter R_d. For both types of nanofluid, the Nusselt number grows with the Prandtl number P_r but decreases with the thermal radiation parameter R_d. Table 5 indicates that the heat production parameter *R* and the thermal slip parameter *C* lower the Nusselt number in both types of nanofluids.

Figure 2a depicts the effects of nanoparticle volume fraction ϕ_0 on the velocity profile of the Cu-water and Al_2O_3 -water nanofluids across the stretching plate. It is fascinating to notice that velocity profiles of Cu-water and Al_2O_3 -water both reduce when ϕ_0 gets a higher value. Figure 2b shows how the nanoparticle volume fraction ϕ_0 affects the temperature profile. We see that when the nanoparticle volume fraction increases in both Cu-water and Al_2O_3-water nanofluids, the temperature profiles climb. The nanoparticles have the physical ability to absorb energy in the form of heat. The temperature rises when more nanoparticles are confined at once because more energy is used. More collisions with suspended nanoparticles produce scatter energy in the form of heat as the number of collisions with particles rises. Figure 2c shows how the velocity parameter for Cu-water andAl_2O_3 -water nanofluid is affected by varying magnetic parameter *M* values. It shows that the hydrodynamic velocity increases as *M* increases. The Lorentzforces provide a greater amount of surface tension. The fluid velocity might increase for the velocity profile as a result of this increased magnetic field, producing a drag force that operates against the fluid's speed. The velocity profile of both types of nanofluids is amplified by an increase in the porosity parameter *P*, as seen in Figure 2d. The relative graph illustrating how the suction/blowing parameter *S* varies and affects velocity fields for Cu-water and Al_2O_3 -water nanofluid is shown in Figure 2e. We see that velocity decreases for both kinds of nanofluids in Figure 2e. This is because the flow approaches the boundary layer as mass suction increases. Consequently, the velocity boundary layer's thickness assumes the form of a thinner layer.

As seen in Figure 2f, the medium's porosity and drag coefficient increase with the Forchheimer number, creating greater resistive forces and decreasing fluid velocity for both Cu-water and Al_2O_3 -water nanofluid. When the first-order and second-velocity slip parameters (*A* and *B*) are increased, the velocity profiles are decreased for the hybrid nanofluid, as shown in Figures 2g-h. It can be shown that for both types of nanofluids, the velocity profile must decrease close to the sheet's surface while increasing away from it as the first and second-order slip parameters rise. Physically, more flow can slide through the surface and increase flow velocity when slip velocity across the stretched sheet's border lowers flow resistance. In order to increase the flow velocity, a high degree of velocity slip is necessary, and vice versa. For water-based Cu and Al_2O_3 nanoparticles, Figure 2i shows the impact of the thermal slip parameter *C* throughout the temperature profile. We find that when the thermal slip parameter *C* increases, the temperature profiles decrease. If thermal slip is managed properly, the necessary heat transfer performance may be achieved.

The effects of the heat production parameter *R* on the temperature profile of two different kinds of nanofluid are shown in Figure 2j. As the heat production parameter increases, so does the fluid temperature. Conduction of heat from the surface into the fluid is physically accelerated by an increase in heat-generating characteristics brought on by a temperature increase. Figure 2k illustrates how the temperature field of both Cu-water and Al_2O_3-water nanofluid is affected by thermal radiation R_d. According to this figure, a higher estimate of R_d causes the fluid temperature to increase, and the physical basis for its increased thermal radiation suggests Rosseland radiative absorptive K^* diminutions. Consequently, the radiative heat flux intensifies the thickness of the thermal boundary layer. As the Prandtl number P_r for both nanofluids increases, the temperature profile decreases, which can be seen in Figure 2m. The thermal boundary layer becomes thinner as the Prandtl number rises. Momentum diffusivity divided by thermal diffusivity is known as the Prandtl number. The relative thickness of the momentum and thermal boundary layers in heat transfer issues is governed by P_r.

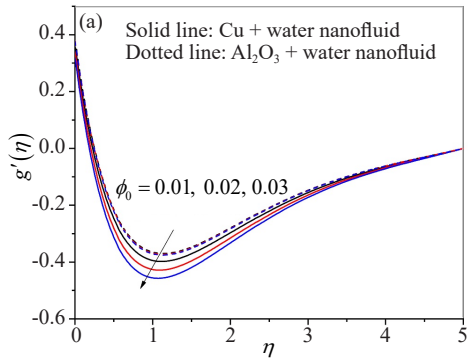
(a)
Solid line: Cu + water nanofluid
Dotted line: Al_2O_3 + water nanofluid
ϕ_0 = 0.01, 0.02, 0.03
$g'(\eta)$
η

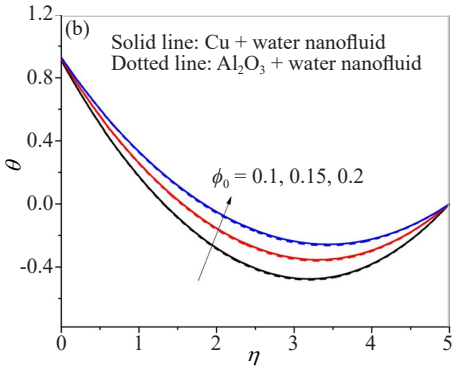
(b)
Solid line: Cu + water nanofluid
Dotted line: Al_2O_3 + water nanofluid
ϕ_0 = 0.1, 0.15, 0.2
θ
η

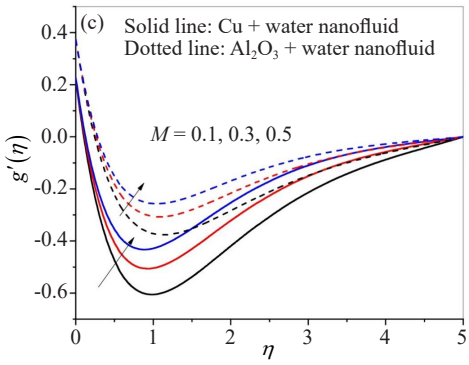
(c)
Solid line: Cu + water nanofluid
Dotted line: Al_2O_3 + water nanofluid
M = 0.1, 0.3, 0.5
$g'(\eta)$
η

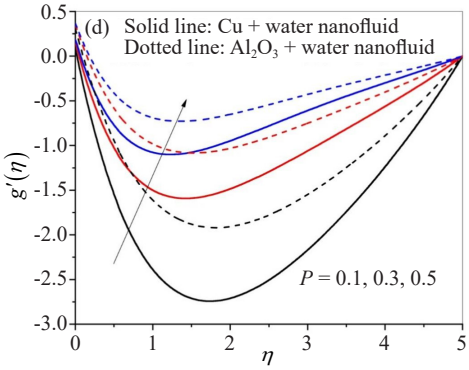
(d)
Solid line: Cu + water nanofluid
Dotted line: Al_2O_3 + water nanofluid
P = 0.1, 0.3, 0.5
$g'(\eta)$
η

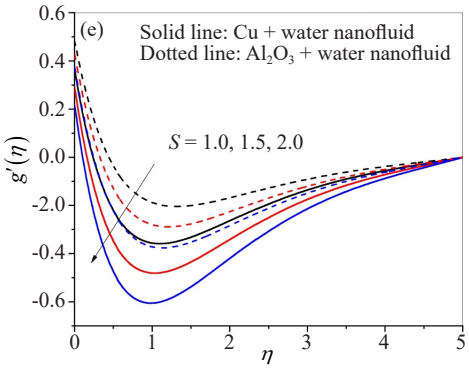
(e)
Solid line: Cu + water nanofluid
Dotted line: Al_2O_3 + water nanofluid
S = 1.0, 1.5, 2.0
$g'(\eta)$
η

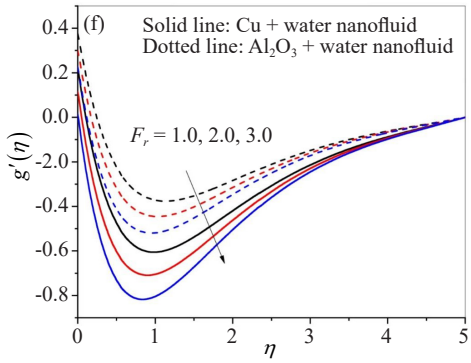
(f)
Solid line: Cu + water nanofluid
Dotted line: Al_2O_3 + water nanofluid
F_r = 1.0, 2.0, 3.0
$g'(\eta)$
η

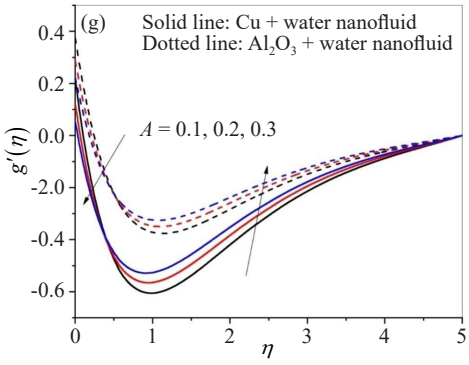
(g)
Solid line: Cu + water nanofluid
Dotted line: Al_2O_3 + water nanofluid
A = 0.1, 0.2, 0.3
$g'(\eta)$
η

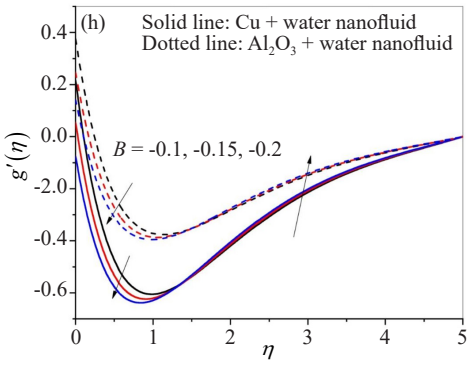
(h)
Solid line: Cu + water nanofluid
Dotted line: Al_2O_3 + water nanofluid
B = -0.1, -0.15, -0.2
$g'(\eta)$
η

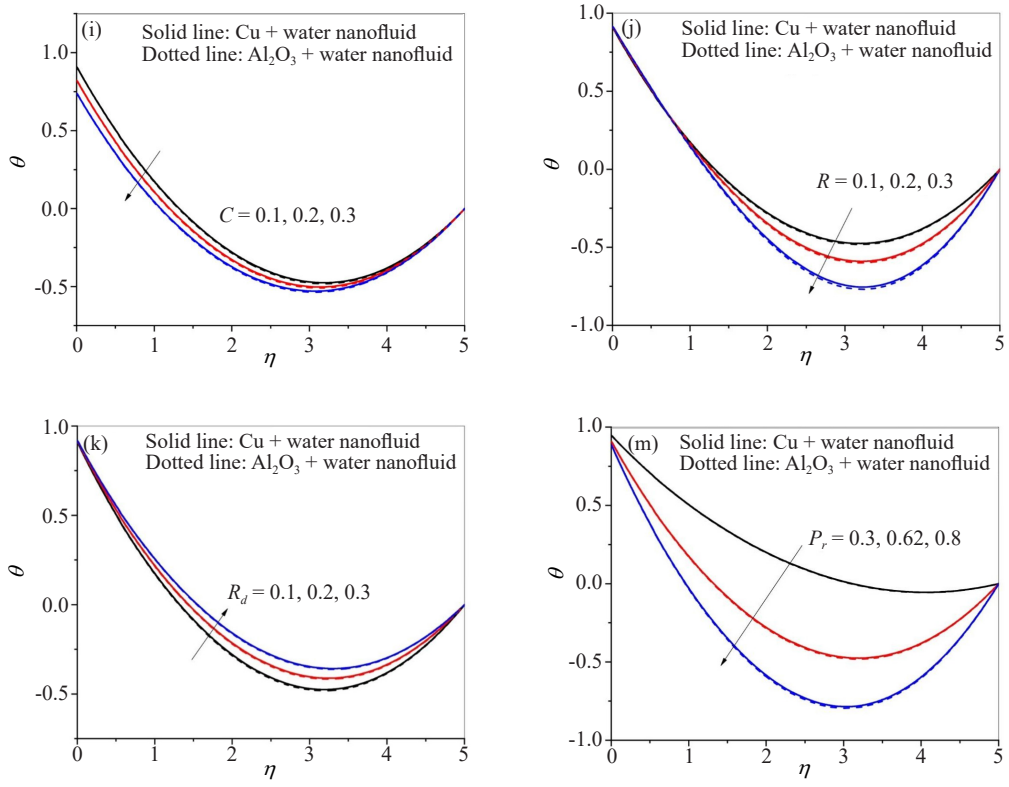

Figure 2. Velocity and temperature profiles against ηfor different values of parameters

6. Conclusions

This paper discusses the flow and heat transfer analysis of Cu-water and Al_2O_3-water nanofluid in an external magnetic field, thermal radiation, and heat production caused by an exponentially stretched surface. Second-order velocity slip and thermal slip are also considered boundary conditions. Similarity transformations convert the governing partial differential equations into a collection of nonlinear ordinary ones. A homotopy perturbation technique is used to obtain analytical solutions for that system of equations. A graphic discussion of the velocity and temperature expressions has been presented.

The following findings have been discovered:

(i) The local Nusselt number increases as the Prandtl number increases, although the thermal radiation parameter shows the opposite tendency. For both varieties of nanofluid, the local Nusselt number is decreased by raising the heat source and thermal radiation.

(ii) The suction parameter augments, but the magnetic field and porous parameter decline the skin friction coefficient.

(iii) The increment of the magnetic field, first and second-order velocity parameters, and porous parameters intensifies the fluid velocity. Still, it diminishes the suction parameter and Forchheimer number for both types of nanofluid.

(iv) The temperature profile can enhance the thermal radiation parameter, but it diminished with the increment of thermal slip and heat source parameter.

(vi) Nanoparticle volume fraction increases the temperature profile for both kinds of nanofluid, but it reduces the velocity profile of both Cu-water and Al_2O_3-water nanofluid.

The present work can further be extended to include mass transfer with chemical reaction, non-uniform heat/source-sink, and many other advanced features in the boundary layer flow problems.

7. Applications

There are important applications in engineering, chemistry, and physics. Examples include metallurgy, which employs hydro-magnetic methods, and the polymer industry, which deals with the stretching of plastic sheets. More specifically, many metallurgical processes include dragging continuous strips or filaments through a quiescent fluid to cool them; sometimes, the drawing process involves stretching the strips. One may discuss drawing, annealing, and thinning copper wire. In each of these cases, the desired feature and the rate at which such strips are cooled in an electrically conducting fluid exposed to a magnetic field have a significant impact on the final product's properties. Additionally, nanofluids are employed in heat exchangers, solar water heating, biomedicine, microelectronic chip cooling, diesel engine productivity enhancement, and automobile engine freezing.

Conflict of interest

The authors declare that they have no conflict of interest.

References

[1] Sakiadis, B. C. Boundary-layer behavior on continuous solid surfaces: II. The boundary layer on a continuous flat surface. *AICHE Journal* **1961,** *7*(2), 221-225.

[2] Tsou, F. K.; Sparrow, E. M.; Goldstein, R. J. Flow and heat transfer in the boundary layer on a continuous moving surface. *Int. J. Heat Mass Transf.* **1967,** *10*(2), 219-235.

[3] Crane, L. J. Flow past a stretching plate. *Zeitschrift fur Angewandte Mathematik und Physik ZAMP.* **1970,** *21*, 645-647.

[4] Pal, D.; Mandal, G. Thermal radiation and MHD effects on boundary layer flow of micropolar nanofluid past a stretching sheet with nonuniform heat source/sink. *Int. J. Mech. Sci*. **2017,** *126*, 308-318.

[5] Mandal, G.; Pal, D. Novel treatments for the radiative-magnetive Ellis hybrid nanofluids flow inside stenotic shrinking artery with imposed convective slip boundary conditions and entropy generation: An application in cardiovascular disease. *Hybrid Advances* **2024,** *7*, 100273.

[6] Mandal, G. Convective-radiative heat transfer of micropolar nanofluid over a vertical non-linear stretching sheet. *J. Nanofluids*. **2016,** *5*(6), 852-860.

[7] Mandal, G.; Pal, D. Impact of gold and silver nanoparticles on the thermally radiating MHD slip blood flow within the stenotic artery using stability analysis and entropy optimisation. *Pramana* **2024,** *98*(4), 1-19.

[8] Choi, S. U.; Eastman, J. A. *Enhancing Thermal Conductivity of Fluids with Nanoparticles*; Argonne National Lab, Argonne, IL (United States), 1995.

[9] Tiwari, R. K.; Das, M. K. Heat transfer augmentation in a two-sidedlid-driven differentially heated square cavity utilizing nanofluids. *Int. J. Heat Mass Transf*. **2007,** *50*(9-10), 2002-2018.

[10] Magyari, E.; Keller, B. Heat and mass transfer in the boundary layers on an exponentially stretching continuous surface. *Journal of Physics D: Applied Physics* **1999,** *32*(5), 577.

[11] Zhang, K.; Shah, N. A.; Alshehri, M.; Alkarni, S.; Wakif, A.; Eldin, S. M. Water thermal enhancement in a porous medium via a suspension of hybrid nanoparticles: MHD mixed convective Falkner's-Skan flow case study. *Case Stud. Therm. Eng.* **2023,** *47*, 103062.

[12] Sajjan, K.; Shah, N. A.; Ahammad, N. A.; Raju, C. S. K.; Kumar, M. D.; Weera, W. Nonlinear Boussinesq and Rosseland approximations on 3D flow in an interruption of Ternary nanoparticles with various shapes of densities and conductivity properties. *AIMS Math* **2022,** *7*(10), 18416-18449.

[13] Rehman, S. U.; Fatima, N.; Ali, B.; Imran, M.; Ali, L., Shah, N. A.; Chung, J. D. The Casson dusty nanofluid: Significance of Darcy-forchheimer law, magnetic field, and non-Fourier heat flux model subject to stretch surface. *Mathematics* **2022,** *10*(16), 2877.

[14] Kumar, M. D.; Raju, C. S. K.; Sajjan, K.; El-Zahar, E. R.; Shah, N. A. Linear and quadratic convection on 3D flow with transpiration and hybrid nanoparticles. *Int. Commun. Heat Mass Transf*. **2022,** *134*, 105995.

[15] Raju, C. S. K.; Ahammad, N. A.; Sajjan, K.; Shah, N. A.; Yook, S. J.; Kumar, M. D. Nonlinear movements of axisymmetric ternary hybrid nanofluids in a thermally radiated expanding or contracting permeable Darcy Walls

with different shapes and densities: Simple linear regression. *Int. Commun. Heat Mass Transf.* **2022,** *135*, 106110.
[16] Merkin, J. H.; Rohni, A. M.; Ahmad, S.; Pop, I. On the temperature slip boundary condition in a mixed convection boundary-layer flow in a porous medium. *Transport in Porous Media* **2012,** *94*(1), 133-147.
[17] Fang, T.; Yao, S.; Zhang, J.; Aziz, A. Viscous flow over a shrinking sheet with a second order slip flow model. *Commun. Nonlinear Sci. Numer. Simul.* **2010,** *15*(7), 1831-1842.
[18] Turkyilmazoglu, M. Heat and mass transfer of MHD second order slip flow. *Computers and Fluids* **2013,** *71*, 426-434.
[19] Sharma, R.; Ishak, A.; Pop, I. Second order slip flow of cu-water nanofluid over a stretching sheet with heat transfer. *WSEAS Trans. Fluid Mech.* **2014,** *9*, 26-33.
[20] Hafidzuddin, E. H.; Nazar, R.; Arifin, N. M.; Pop, I. Boundary layer flow and heat transfer over a permeable exponentially stretching/shrinking sheet with generalized slip velocity. *J. Appl. Fluid Mech*. **2016,** *9*(4), 2025-2036.
[21] Laxmi, T. V.; Shankar, B. Radiative boundary layer flow and heat transfer of nanofluid over a nonlinear stretching sheet with slip conditions and suction. *Jordan J. Mech. Ind. Eng.* **2016,** *10*(4), 285-297.
[22] Mabood, F.; Shateyi, S. Multiple slip effects on MHD unsteady flow heat and mass transfer impinging on permeable stretching sheet with radiation. *Mod. Simul. Eng.* **2019,** *2019*(1), 3052790.
[23] Amos, E.; Uka, U. A. Hydromagnetic nanofluid flow over an exponentially stretching sheet in the presence of radiation and nonuniform heat generation. *IOSR Journal of Mathematics*. **2022,** *18*(1), 31-43.
[24] Kaushik, P.; Mishra, U. Second-Order slip effect on MHD flow and radiative heat transfer through porous medium due to an exponentially stretching sheet. *Trends Sci*. **2022,** *19*(15), 5612.
[25] He, J. H. Homotopy perturbation technique. *Comput. Methods Appl. Mech. Eng.* **1999,** *178*(3-4), 257-262.
[26] He, J. H. Homotopy perturbation method: A new nonlinear analytical technique. *Appl. Math Comput*. **2003,** *135*(1), 73-79.
[27] He, J. H. Homotopy perturbation method for bifurcation of nonlinear problems. *Commun. Nonlinear Sci. Numer. Simul*. **2005,** *6*(2), 207-208.
[28] El-dabe, N. T.; Abou-zeid, M. Y.; Ahmed, O. S. Motion of a thin film of a fourth grade nanofluid with heat transfer down a vertical cylinder: Homotopy perturbation method application. *Journal of Advanced Research in Fluid Mechanics and Thermal Sciences* **2020,** *66*(2), 101-113.
[29] Abou-Zeid, M. Y. Homotopy perturbation method for couple stresses effect on MHD peristaltic flow of a non-Newtonian nanofluid. *Microsystem Technologies* **2018,** *24*(12), 4839-4846.
[30] Jhankal, A. K. Homotopy perturbation method for MHD boundary layer flow with low pressure gradient over a flat plate. *J. Appl. Fluid Mech.* **2014,** *7*(1), 177-185.
[31] Sarma, M. K.; Sinha, S.; Das, B. Homotopy perturbation method for MHD boundary layer flow over a moving vertical plate in presence of heat and mass transfer. *South East Asian J. Math. Math. Sci*. **2020,** *16*(3), 269.
[32] Kumar, M. D.; Ahammad, N. A.; Raju, C. S. K.; Yook, S. J.; Shah, N. A.; Tag, S. M. Response surface methodology optimization of dynamical solutions of Lie group analysis for nonlinear radiated magnetized unsteady wedge: Machine learning approach (gradient descent). *Alex. Eng. J.* **2023,** *74*, 29-50.
[33] Wahid, N. S.; Arifin, N. M.; Khashi'ie, N. S.; Pop, I. Hybrid nanofluid slip flow over an exponentially stretching/shrinking permeable sheet with heat generation. *Mathematics* **2020,** *9*(1), 30.
[34] Yan, L.; Dero, S.; Khan, I.; Mari, I. A.; Baleanu, D.; Nisar, K. S.; Sherif, E. S. M.; Abdo, H. S. Dual solutions and stability analysis of magnetized hybrid nanofluid with joule heating and multiple slip conditions. *Processes* **2020,** *8*(3), 332.
[35] Magyari, E.; Pantokratoras, A. Note on the effect of thermal radiation in the linearized Rosseland approximation on the heat transfer characteristics of various boundary layer flows. *Int. Commun. Heat Mass Transf.* **2011,** *38*(5), 554-556.
[36] Eid, M. R.; Nafe, M. A. Thermal conductivity variation and heat generation effects on magneto-hybrid nanofluid flow in a porous medium with slip condition. *Waves Random Complex Media* **2022,** *32*(3), 1103-1127.
[37] Mandal, G. Smoluchowski temperature and Maxwell velocity slip impacts on magneto-radiative Fe_3O_4-Al_2O_3-Cu/H_2O tri-hybrid nanofluid flow over a shrinking surface with entropy generation: a stability performance. *IJMS* **2024,** 1-28.
[38] Ali, A.; Noreen, A.; Saleem, S.; Aljohani, A. F.; Awais, M. Heat transfer analysis of Cu-Al_2O_3 hybrid nanofluid with heat flux and viscous dissipation. *J. Therm. Anal. Calorim.* **2021,** *143*(3), 2367-2377.

Appendix

$$A_{21}=\frac{\mu_{nf}}{\mu_f},\ A_{22}=\frac{\rho_{nf}}{\rho_f},\ A_2=\frac{A_{21}}{A_{22}},\ A_{31}=\frac{\sigma_{nf}}{\sigma_f},\ A_3=\frac{A_{31}}{A_{22}},\ A_4=\frac{1}{A_2},\ E_1=\frac{2}{A_2}+\frac{F_r}{A_2},\ F_1=\frac{A_3M}{A_2}+P,$$

$$A_5=\frac{1}{P_r}\left(\frac{\kappa_{nf}}{\kappa_f}+R_d\right),\ A_6=\frac{\left(\rho c_p\right)_{nf}}{\left(\rho C_p\right)_f},\ L_1=\frac{A_6}{A_5},\ L_2=\frac{R}{A_5},\ h_1=-\sqrt{F_1}-AF_1+BF_1^{3/2},$$

$$h_2=+\sqrt{F_1}-AF_1-BF_1^{3/2},\ h_3=-\sqrt{F_1}e^{-5\sqrt{F_1}},\ h_4=\sqrt{F_1}e^{5\sqrt{F_1}},\ d_2=\frac{h_4}{h_1h_4-h_2h_3},\ d_3=\frac{h_3}{h_1h_3-h_1h_4},$$

$$d_1=S-d_2-d_3,\ h_5=A_4d_1d_2F_1,\ h_6=A_4d_1d_3F_1,\ h_7=\left(A_4-E_1\right)d_2^2F_1,\ h_8=\left(A_4-E_1\right)d_2^3F_1,$$

$$h_9=2d_2d_3E_1F_1,\ h_{10}=\frac{h_5}{2F_1},\ h_{11}=\frac{h_6}{2F_1},\ h_{12}=\frac{h_7}{6F_1^{3/2}},\ h_{13}=\frac{h_8}{6F_1^{3/2}},\ h_{14}=\frac{h_9}{F_1},\ h_{15}=-h_{12}+h_{13},$$

$$h_{16}=2h_{10}\sqrt{F_1}-2h_{11}\sqrt{F_1}+4h_{12}F_1-4h_{13}F_1,\ h_{17}=-h_{10}-h_{11}-2h_{12}\sqrt{F_1}-2h_{13}\sqrt{F_1}+h_{14},$$

$$h_{18}=-3h_{10}F_1-3h_{11}F_1-8h_{12}F_1^{3/2}-h_{13}F_1^{3/2},\ h_{19}=h_1,\ h_{20}=h_2,\ h_{21}=Ah_{16}+Bh_{18}-h_{17},\ h_{22}=-\sqrt{F_1}e^{-5\sqrt{F_1}},$$

$$h_{23}=\sqrt{F_1}e^{5\sqrt{F_1}},\ h_{24}=-h_{10}e^{-5\sqrt{F_1}}+5h_{10}\sqrt{F_1}e^{-5\sqrt{F_1}}-h_{11}e^{5\sqrt{F_1}}-5h_{11}\sqrt{F_1}e^{5\sqrt{F_1}}-2h_{12}\sqrt{F_1}e^{-10\sqrt{F_1}}-2h_{13}\sqrt{F_1}e^{10\sqrt{F_1}}+h_{14},$$

$$d_5=\frac{h_{23}h_{21}+h_{20}h_{24}}{h_{23}h_{19}+h_{22}h_{20}},\ d_6=\frac{h_{22}h_{21}-h_{24}h_{19}}{h_{22}h_{20}+h_{19}h_{23}},\ d_4=h_{15}-d_5-d_6,\ d_7=\frac{\sin\left(5\sqrt{L_2}\right)}{c\sqrt{L_2}\,\mathrm{Cos}\left(5\sqrt{L_2}\right)+\sin\left(5\sqrt{L_2}\right)},$$

$$d_8=\frac{\cos\left(5\sqrt{L_2}\right)}{c\sqrt{L_2}\,\mathrm{Cos}\left(5\sqrt{L_2}\right)+\mathrm{Sin}\left(5\sqrt{L_2}\right)},\ d_{11}=L_1d_1d_7\sqrt{L_2},\ d_{12}=-L_1d_1d_8\sqrt{L_2},$$

$$d_{13}=\left(d_7\sqrt{L_2}-d_8\sqrt{F_1}\right)L_1d_2,\ d_{14}=-\left(d_8\sqrt{L_2}+d_7\sqrt{F_1}\right)L_1d_2,\ d_{15}=\left(d_7\sqrt{L_2}+d_8\sqrt{F_1}\right)L_1d_3,$$

$$d_{16}=-\left(d_8\sqrt{L_2}-d_7\sqrt{F_1}\right)L_1d_3,\ d_{17}=\frac{2d_{13}\sqrt{L_2}}{\sqrt{F_1}\left(4L_2+F_1\right)},\ d_{18}=\frac{d_{13}}{4L_2+F_1},\ d_{19}=-\frac{2d_{14}\sqrt{L_2}}{\sqrt{F_1}\left(4L_2+F_1\right)},$$

$$d_{20}=\frac{d_{14}}{4L_2+F_1},\ d_{21}=-\frac{2d_{15}\sqrt{L_2}}{\sqrt{F_1}\left(4L_2+F_1\right)},\ d_{22}=\frac{d_{15}}{4L_2+F_1},\ d_{23}=\frac{2d_{16}\sqrt{L_2}}{\sqrt{F_1}\left(4L_2+F_1\right)},\ d_{24}=\frac{d_{16}}{4L_2+F_1},$$

$$d_{25}=-\frac{d_{11}}{2\sqrt{L_2}},\ d_{26}=\frac{d_{12}}{2\sqrt{L_2}},\ d_{27}=d_{17}+d_{20},\ d_{28}=d_{18}+d_{19},\ d_{29}=d_{21}+d_{24},\ d_{30}=d_{22}+d_{23},$$

$$d_{31} = c\left(d_{25} - d_{27}\sqrt{F_1} + d_{28}\sqrt{L_2} + d_{29}\sqrt{F_1} + d_{30}\sqrt{L_2}\right) - d_{27} - d_{29},$$

$$d_{32} = 5d_{25}\,\mathrm{Cos}\left(5\sqrt{L_2}\right) + 5d_{26}\,\mathrm{Sin}\left(5\sqrt{L_2}\right),$$

$$d_{33} = d_{27}e^{-5\sqrt{F_1}}\,\mathrm{Cos}\left(5\sqrt{L_2}\right) + d_{28}e^{-5\sqrt{F_1}}\,\mathrm{Sin}\left(5\sqrt{L_2}\right),$$

$$d_{34} = d_{29}e^{5\sqrt{F_1}}\,\mathrm{Cos}\left(5\sqrt{L_2}\right) + d_{30}e^{5\sqrt{F_1}}\,\mathrm{Sin}\left(5\sqrt{L_2}\right),$$

$$d_{35} = -\left(d_{32} + d_{33} + d_{34}\right),\ d_9 = \frac{d_{31}\,\mathrm{Sin}\left(5\sqrt{L_2}\right) + d_{35}c\sqrt{L_2}}{\mathrm{Sin}\left(5\sqrt{L_2}\right) + c\sqrt{L_2}\,\mathrm{Cos}\left(5\sqrt{L_2}\right)},\ d_{10} = \frac{d_9 - d_{31}}{c\sqrt{L_2}}$$